Robust Power Control of Microgrid based on Hybrid Renewable Power Generation Systems

Amin Hajizadeh[1]

1. Department of Electrical Engineering, Shahrood University of Technology, Shahrood, Iran.

.

Abstract

This paper presents modeling and control of a hybrid distributed energy sources including photovoltaic (PV), fuel cell (FC) and battery energy storage (BES) in a microgrid which provides both real and reactive power to support an unbalanced utility grid. The overall configuration of the microgrid including dynamic models for the PV, FC, BES and its power electronic interfacing are briefly described. Then controller design methodologies for the power conditioning units to control the power flow from the hybrid power plant to the unbalanced utility grid are presented. In order to distribute the power between power sources, the neuro-fuzzy power controller has been developed. Simulation results are presented to demonstrate the effectiveness and capability of proposed control strategy.

Keywords: Microgrid, Power Control, Renewable energy, Fuel Cell, Photovoltaic, Energy Storage

1. Introduction

Integration of distributed energy resources (DER) units with energy storages has brought about the concept of microgrid [1-3]. A microgrid is defined as a cluster of energy sources include wind turbine, photovoltaic, fuel cell and loads, serviced by a distribution system, and can operate in the grid-connected mode, the islanded (autonomous) mode and ride-through between the two modes [4].

Combining the non-dispatchable renewable energy sources, like solar energy with dispatchable energy sources like fuel cell and energy storage make the best use of the advantages of each individual device [5]. Hybridization of fuel cell with PV will therefore form a very reliable distributed generation where the fuel cell acts as back up during low PV output [6]. The energy storage can be used to supply high transient energy and thus greatly improve system dynamics [7]. A microgrid can be strategically placed at any site in a power system (normally at the distribution level) for grid reinforcement, thereby deferring or eliminating the need for system upgrades and improving system integrity, reliability, and efficiency.

When connected to a utility grid, important operation and performance requirements are imposed on microgrid.

The main challenge in operating such hybrid system is the coordination of the numerous generators for sharing the real and reactive power output and the control of system frequency and voltage.

Up to now many studies have been presented for control and management of microgrid. Some of them have concentrated on the operation of control strategies in microgrid [8-10]. In these researches, the modeling of microgrid and implementation of control strategies have not been considered. In other investigations, only the control of power electronic converters in microgrid has been discussed [11-14].

However, in order to power control of microgrid it is necessary to study the whole system with considering the dynamical and physical properties of each power sources in microgrid and the power electronic converters.

Hence, in this paper, power management strategy of a microgrid in grid connected mode is introduced. First, dynamic model of hybrid renewable energy sources in a microgrid is presented.

The hybrid power plant is interfaced with the utility grid via boost dc/dc converters and a three-phase pulsewidth modulation (PWM) inverter. The models for the boost dc/dc converter and the three-phase inverter together are also addressed. The overall aim is to split the active power flow between hybrid power sources and control of active and reactive power of this microgrid while taking into account component and system constraints. A control strategy for reliable power sharing between power sources in the microgrid is proposed and simulation results are shown with real and reactive power control capability.

2. Proposed Structure of Microgrid based on Hybrid Renewable Power Sources

The dynamic modeling of Hybrid Renewable Power Sources (HRPS) system is an important issue that needs to be carefully addressed. To study the performance characteristics of HRPS systems, accurate models of fuel cell, photovoltaic and battery energy storage are needed. Moreover, models for the interfacing power electronic circuits in a HRPS system are also needed to design controllers for the overall system to improve its performance and to meet certain operation requirements. To meet the system operational requirements, a HRPS system needs to be interfaced through a set of power electronic devices. Fig.1 shows the block diagram of the HRPS proposed in this paper that connected to main grid in Point Common Coupling (PCC). The mathematical models describing the dynamic behavior of each of these components are given below.
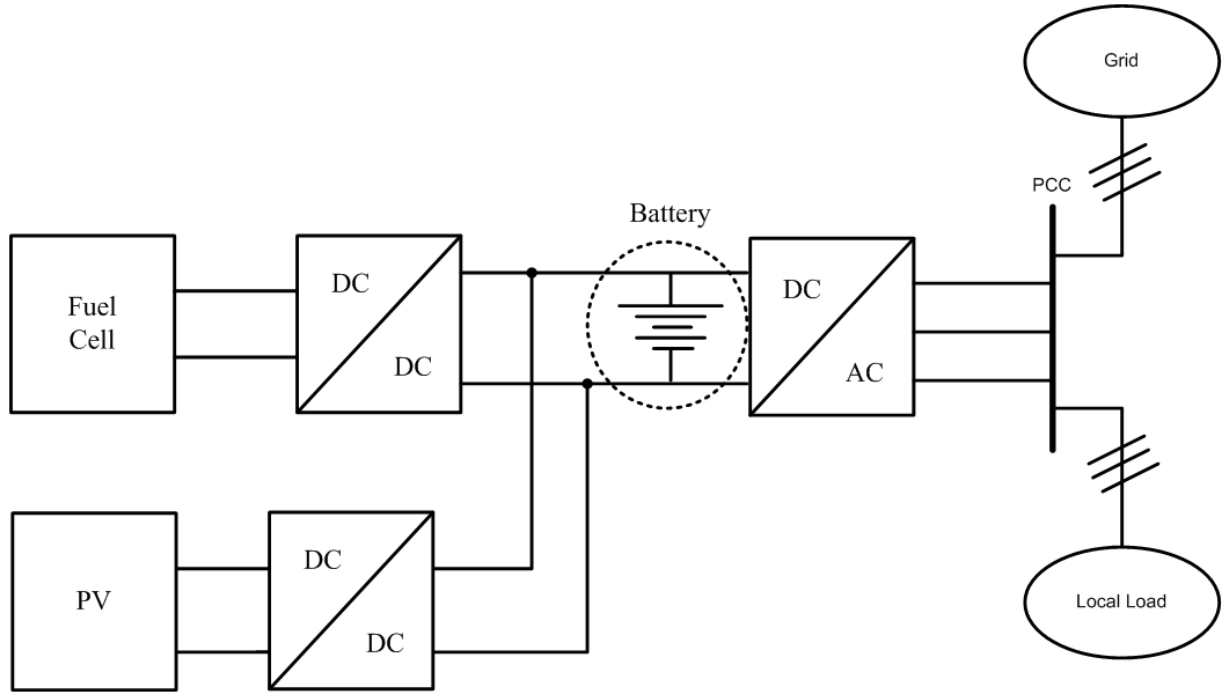
Fig 1: Hybrid Renewable energy sources in a microgrid

2.1. Fuel Cell Model

Fuel cells are static energy conversion devices that convert the chemical energy of fuel directly into electrical energy. The model of fuel cell power plant used in this study is based on the dynamic PEMFC stack model developed in [16]. The performance of fuel cell is affected by several operating variables, as discussed in the following. This model is based on simulating the relationship between output voltage and partial pressure of hydrogen, oxygen, and water. The Nernst's equation and Ohm's law determine the average voltage magnitude of the fuel cell stack. The following equation shows the voltage of the fuel cell stack:

$$V_{fc} = N_0 (E_0 + \frac{RT}{2F}(\log(\frac{P_{H_2} P_{O_2}^{0.5}}{P_{H_2O}})) - R_{int}I \tag{1}$$

Where:

N_0 is the number of cells connected in series;

R_{int} is the internal resistance of fuel cell stack [Ω]

E_0 is the voltage associated with the reaction free energy;

R is the universal gas constant;

T is the temperature;

3

I is the current of the fuel cell stack;

F is the Faraday's constant.

P_{H2}, P_{H2O}, P_{O2} are determined by the following differential equations:

$$\dot{P}_{H_2} = -\frac{1}{t_{H_2}}(P_{H_2} + \frac{1}{K_{H_2}}(q_{H_2}^{in} - 2K_r I_{fc}))$$

$$\dot{P}_{H_2O} = -\frac{1}{t_{H_2O}}(P_{H_2O} + \frac{2}{K_{H_2O}}K_r I_{fc})) \tag{2}$$

$$\dot{P}_{O_2} = -\frac{1}{t_{O_2}}(P_{O_2} + \frac{1}{K_{O_2}}(q_{O_2}^{in} - K_r I_{fc}))$$

Where, $q_{H_2}^{in}$ and $q_{O_2}^{in}$ are the molar flow of hydrogen and oxygen and where the K_r constant is defined by the relation between the rate of reactant hydrogen and the fuel cell current:

$$q_{H_2}^{r} = \frac{N_0 I}{2F} = 2K_r I \tag{3}$$

Moreover, a simple model of reformer that generates hydrogen through methane has been considered. The model is second-order transfer function. The mathematical form of the model can be written as follows:

$$\frac{q_{H_2}}{q_{methane}} = \frac{CV}{\tau_1 \tau_2 s^2 + (\tau_1 + \tau_2)s + 1} \tag{4}$$

Where

$q_{methane}$ is methane flow rate [kmol/sec];

CV   is conversion factor [kmol of hydrogen per kmol of methane];

τ_1, τ_2 are reformer time constants [sec].

2.2. Photovoltaic Model

The photovoltaic arrays (PVs) are an attractive source of renewable energy for distributed urban power generation due to their relatively small size and noiseless operation. Their applications are expected to significantly increase all over the world. The most common PV model used is the one diode model. The model used in this paper is the one diode model whose equivalent circuit is shown in Fig.2. An initial understanding of the performance of a solar cell may be obtained by considering it as a diode. The light energy, which is in the form of photons with the appropriate energy level, falls on the cell and generates electron-hole pairs. The electrons and holes are separated by the electric field established at the junction of the diode and are then driven around an external circuit by this junction potential [17].
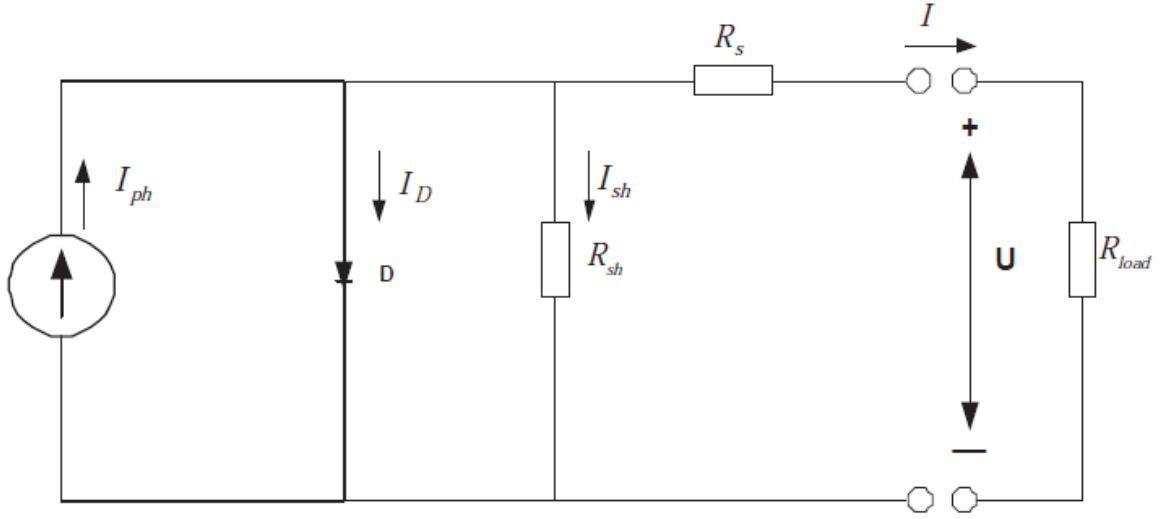
Fig.2.one diode model of PV

The PV cell can be modeled as a diode in parallel with a constant current source and a shunt resistor. These three components are in series with the series resistor. The output terminal current I is equal to the light-generated current I_{ph}, with subtracted diode current I_D and the shunt-leakage current I_{sh}.

$$I = I_{ph} - I_D - I_{sh} \qquad (5)$$

The series resistance Rs represents the internal resistance of the current flow, and it depends on the p-n junction depth, the impurities and the contact resistance. The shunt resistance R_{sh} is inversely related to the leakage current to the ground. In an ideal PV cell, $Rs = 0$ (no series loss), and $R_{sh} = 1$ (no leakage to ground). The PV cell conversion efficiency is sensitive to small variations in R_s, but is insensitive to variations in R_{sh}. A small increase in R_s can decrease the PV output significantly. In the equivalent circuit, the current delivered to the external load equals the current I_{ph} generated by the illumination, less than the diode current I_D and the ground-shunt current I_{sh}. The open circuit voltage U_{oc} of the cell is obtained when the load current is zero, i.e., when $I_{sh} = 0$ and is given as:

$$U_{OC} = U + IR_S \qquad (6)$$

Where, U is the terminal voltage of the cell [V].

The diode current I_D is given by the classical diode current expression [18]:

$$I_D = I_d \left[\frac{qU_{oc}}{A_c f K_B T} - 1 \right] \qquad (7)$$

Where

I_d is the saturation current of the diode,

5

q is electron charge = 1.6×10^{-19} Coulombs,

A_{cf} is curve fitting constant,

K_B is Boltzmann constant = 1.38×10^{-23} Joule/ $^{\circ}$KT

T is   temperature [$^{\circ}$K].

The output current is given by [18]:

$$I = I_{ph} - I_{OS} \left\{ \exp\left[\frac{qU_{OC}}{A_C f K_B T} \right] - 1 \right\} - \frac{U_{OC}}{R_{sh}}$$

(8)

Where:

$$I_{ph} = \frac{G}{100}\left[I_{SCR} + K_I (T - 25) \right]$$

(9)

$$I_{oc} = I_{o\gamma}\left(\frac{T}{T_{\gamma}} \right)^3 \exp\left[\frac{qE_{GO}}{BK_B}\left(\frac{1}{T_{\gamma}} - \frac{1}{T} \right) \right]$$

(10)

Where

I, U	cell output current and voltage,
I_{os}	cell reverse saturation current,
B	ideality factor of p-n junction,
K_I	short circuit current temperature coefficient at I_{SCR}, K_I= 0.0017 $A/°C$,
G	solar irradiation in W/m^2,
I_{SCR}	short circuit current at $25°C$ and $1000W/m2$,
I_{ph}	light generated current
E_{GO}	band gap for silicon,
T_r	reference temperature, T_r=301.18 $^{\circ}K$,
I_{or}	cell saturation current at T_r,
R_{sh}	shunt resistance,
R_s	series resistance.

I_{SCR}, the current at maximum power point (I_{mpp}), the voltage at maximum power point (V_{mpp}), and the open circuit voltage of the cell U_{oc}, are given by the manufacturers.

The photovoltaic module operates at on the V-I characteristics that are determined by the load. Since the power harvested from the photovoltaic module is different at different operating points it is important that the load is matched in such a way that maximum power is obtained from the photovoltaic module [19]. The simplest and widely known algorithm is the perturb and observe algorithm. It works by periodically changing the array terminal voltage and comparing the calculated power with that from the previous samples as shown in Figure 3.11. There are other numerous and more complex and efficient algorithms and a comparative study has been done on these algorithms [20].
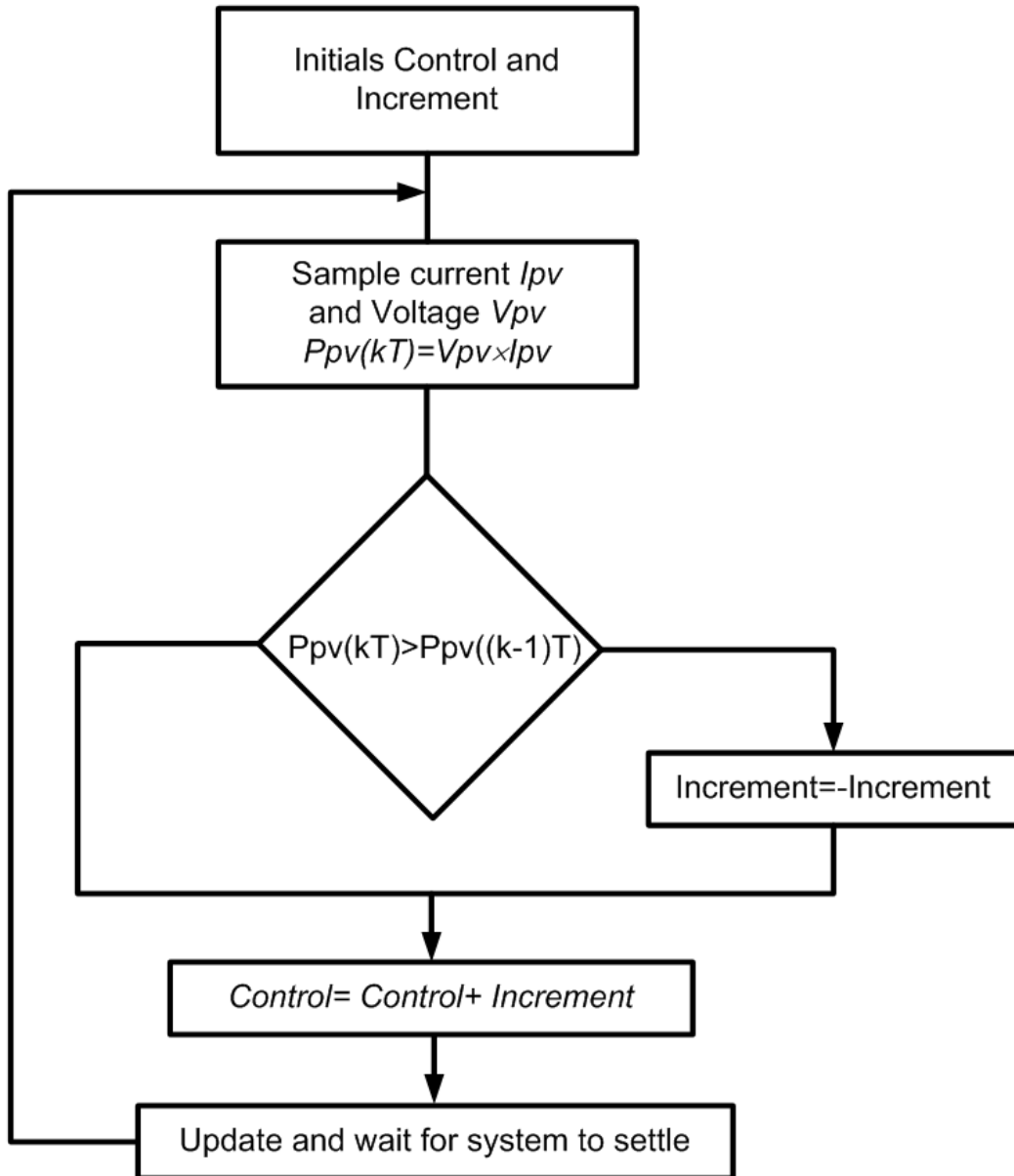
Fig.3 Perturb and observe algorithm for MPPT

2.3. Boost DC/DC Converter Model

The role of boost DC/DC converters is to provide power to the user in a suitable form at high efficiency. Power electronic converters are needed in PV and fuel cell systems to convert DC voltage to the required values. Fig.4 shows the DC/DC converter model. This boost converter is described by the following two non-linear state space averaged equations [21]:
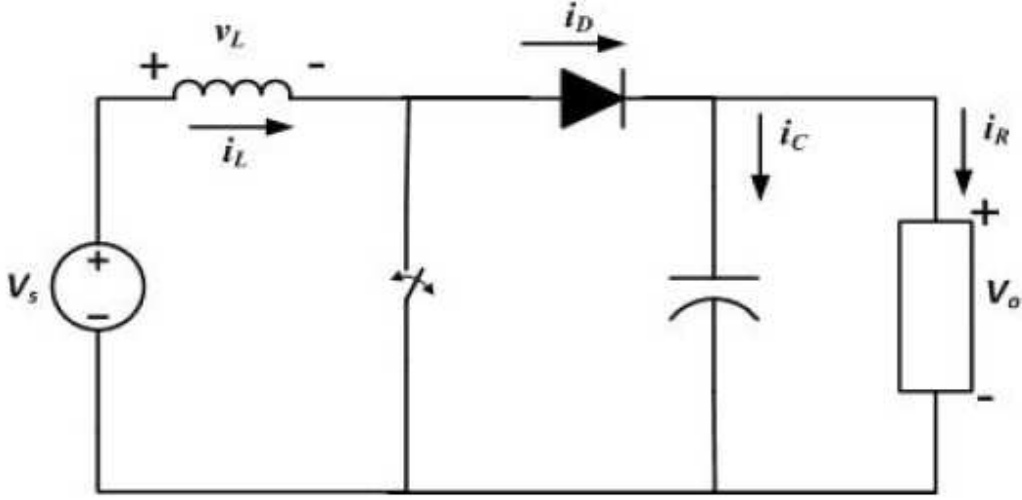
Fig.4. Boost DC/DC Converter Model

$$\frac{di_L}{dt} = -\frac{R_L}{L} - (\frac{1-d}{L})V_o + \frac{1}{L}V_s$$

$$\frac{dV_C}{dt} = \frac{(1-d)}{C}.i_L - \frac{i_R}{C}$$

(11)

Where ''d'' is the duty cycle of the switching device, ''U'' is the input voltage, ''i_L'' is the inductor

current, ''V_C'' is the output voltage and "i_O" is the output current.

2.4. DC-AC Converter Model

A three-phase equivalent circuit of voltage source converter (VSC) is shown in Fig. 8. To reduce

harmonics, LCL filter is connected between the converter and the grid [19]. The dynamic model of the

three-phase VSC is represented in:

$$\frac{di_{1k}}{dt} = -\frac{R_1}{L_1}i_{1k} + \frac{1}{L_1}(v_{ik} - v_{ck})$$

$$\frac{di_{2k}}{dt} = -\frac{R_2}{L_2}i_{2k} + \frac{1}{L_1}(v_{ck} - v_{sk})$$

(14)

$$C_f \frac{dV_{ck}}{dt} = i_{1k} - i_{2k}$$
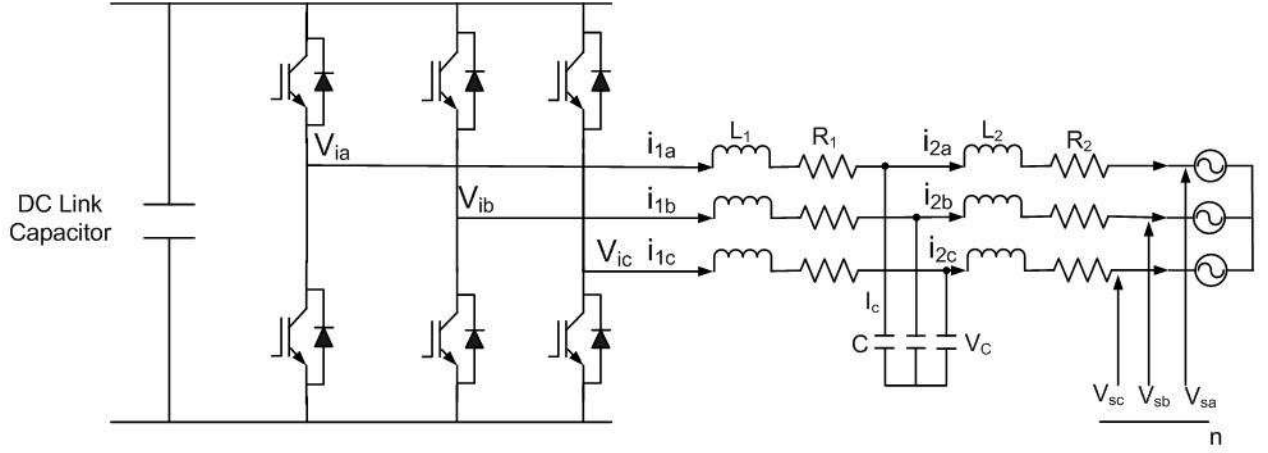
8

Where $k= \{a, b, c\}$.

Fig.5. Three-phase dc/ac voltage source inverter

3. Power Flow Control

Power flow control from hybrid power sources to local AC bus and to/from storage devices is required to maintain power balance at all times while satisfying the active and reactive power demanded by the load. Equation (13) gives power balance expressions that should be satisfied both at the DC-link and at the PCC at all times. The rate and magnitude of fuel cell power P_{FC} and rate, sign and magnitude of battery power P_{Batt} depend on the magnitude and how fast the load changes.

$$P_{MG} = P_{PV} + P_{FC} + P_{Batt}$$
$$P_{Load} = P_{MG} + P_{Grid}$$
$$Q_{Load} = Q_{MG} + Q_{Grid}$$
(14)

According to the control strategy proposed in this paper, P_{Load} and Q_{Load} are made equal to P_{ref} and Q_{ref} so that the hybrid power system output follows the load demand under normal loading conditions and P_{Grid} and Q_{Grid} are zero. If the local load demand exceeds the hybrid power system capacity, the rest of the power is supplied from the grid. Fig.6 shows the overall structure of the control strategy.

The control strategy also keeps the DC-link/battery voltage within a band around the nominal DC-link voltage to keep the inverter in synchronism with the grid.

The following differential equation for DC link power balance is given:

$$C_{dc} v_{dc} \frac{dv_{dc}}{dt} = P_{FC} + P_{PV} + P_{Batt} - P_{Grid}$$
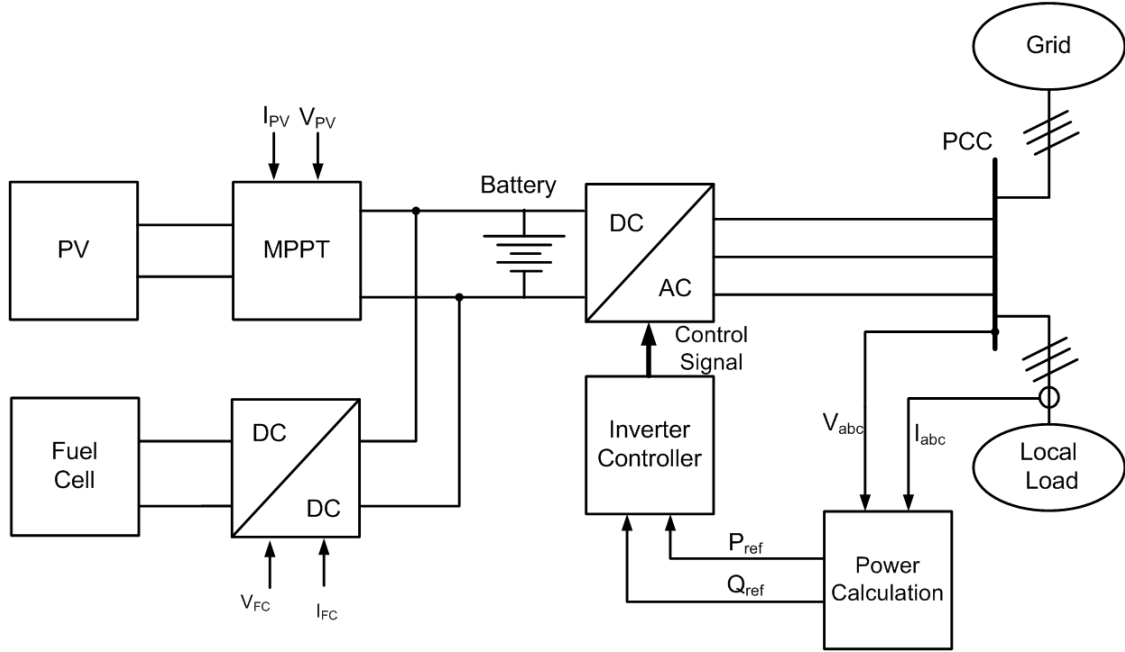(15)

Fig.6. Overall system control structure

According to the equation (31), in order to regulate the dc link voltage it is necessary to keep the power balance in dc link. In this equation, the change in grid power is considered as disturbance during the load power variations. Moreover, to meet the power balance in DC link it is important to consider the dynamic limitations of fuel cell power. In this case, the fuel cell power could not change rapidly and the fuel cell controller with DC-DC converter should regulate the operating point of fuel cell. The details of fuel cell and DC-DC converter control strategy are presented in next part. But the amount of power that should be absorbed by battery energy storage to balance the power in DC link is very important and it depends on the DC link energy. The DC link energy measurement is carried out by means of the following calculation:

$$E_{dc}(k) = (\frac{1}{2})C_{dc}V_{dc}^2(k)$$

(16)

In this paper, a power flow control structure has been developed for hybrid power sources during voltage sag. It is based on fuzzy logic control (FLC) strategy that determines the battery energy storage power according to the following inputs:

$$e(k) = E_{dc-ref}(k) - E_{dc}(k)$$
$$\Delta e(k) = e(k) - e(k-1)$$

(17)

Where E_{dc-ref} is the reference dc link energy which is calculated by reference dc link voltage.

Hence, it is essential to design robust and stable control strategy to guarantee the stability of the dc link of hybrid system. For this purpose, a fuzzy neural control startegy is devloped [22].

10

In proposed neuro-fuzzy control strategy, for each input, four fuzzy subsets have been used. These are ZE (zero), L (low), M (medium) and H (high). For each of these fuzzy sets, a gaussian membership function has been used. As each of the two inputs has four subsets, there are altogether 16 control rules in the neuro-fuzzy logic controller.

The neuro-fuzzy algorithm uses membership functions of gaussian type. With gaussian fuzzy sets, the algorithm is capable of utilizing all information contained in the training set to calculate each rule conclusion, which is different when using triangular partitions. Figure 8 illustrates the neuro-fuzzy scheme for an example with two input variables (x_1, x_2) and one output variable (y). In the first stage of the neuro-fuzzy scheme, the two inputs are codified into linguistic values by the set of gaussian membership functions attributed to each variable. The second stage calculates each rule $R^{(l)}$ its respective activation degree. Last, the inference mechanism weights each rule conclusion $\omega^{(l)}$, initialized by the cluster-based algorithm, using the activation degree computed in the second stage.
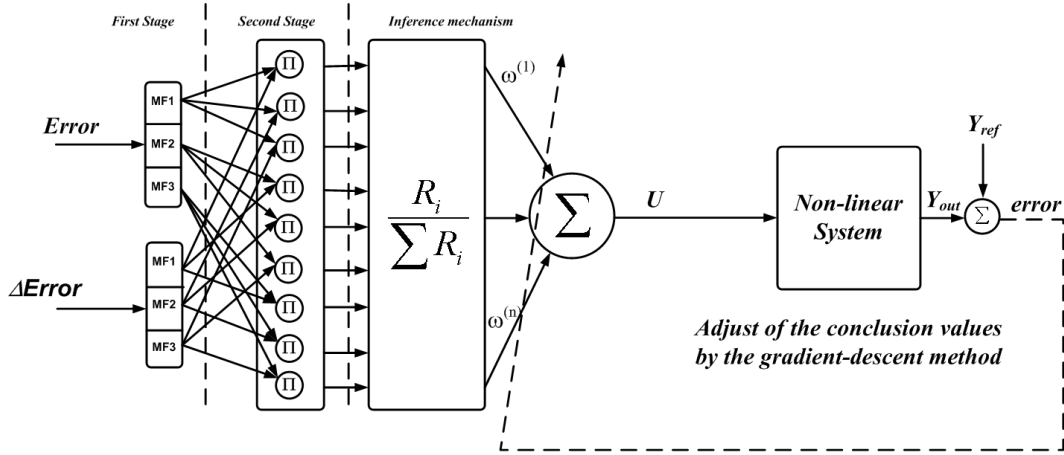

Fig.8. The neuro-fuzzy scheme

The error signal between the model inferred value *Y* and the respective measured value (or teaching value) *y'*, is used by the gradient descent method to adjust each rule conclusion. The algorithm modifies the values of $\omega^{(l)}$ to minimize an objective function *E* usually expressed by the mean quadratic error (15). In this equation, the value *y'(k)* is the desired output value related with the condition vector $x'(k) = (x_1'$, $x_2', \dots x_m')$. The element *Y(x'(k))* is the inferred response to the same condition vector *x'(k)* and computed by Equation (16).

$$E = \frac{1}{2}[Y(x'(k)) - y'(k)]^2 \tag{15}$$

$$Y(x^{'}(k)) = \frac{\sum\limits_{l=1}^{c}\left(\prod\limits_{j=1}^{m}\mu_{A_{j=1}^{(l)}}(x_{j}^{'}(k))\right).\omega^{(l)}(k)}{\sum\limits_{l=1}^{c}\left(\prod\limits_{j=1}^{m}\mu_{A_{j=1}^{(l)}}(x_{j}^{'}(k))\right)} \tag{16}$$

Equation (17) establishes adjustment of each conclusion $\omega^{(l)}$ by the gradient-descent method. The symbol α is the learning rate parameter, and t indicates the number of learning iterations executed by the algorithm.

$$\omega^{(l)}(t+1) = \omega^{(l)}(t) - \alpha\frac{\partial E}{\partial \omega^{(l)}} \tag{17}$$

The inference function (16) depends on $\omega^{(l)}$ only through its numerator. The expression composing the numerator is now denoted by a and is shown in (18).

$$a = \sum\limits_{l=1}^{c}\left(\prod\limits_{j=1}^{m}\mu_{A_{j=1}^{(l)}}(x_{j}^{'}(k))\right).\omega^{(l)}(k) \tag{18}$$

The denominator of function (16) is dependent on a term $d^{(l)}$, defined in (19), and denoted by b in (20).

$$d^{(l)} = \prod\limits_{j=1}^{m}\mu_{A_{j=1}^{(l)}}(x_{j}^{'}(k)) \tag{19}$$

$$b = \sum\limits_{l=1}^{c}(d^{(l)}) \tag{20}$$

To calculate the adjustment of each conclusion value $\omega^{(l)}$, it is necessary to compute the variation of the objective function E, ∂E, in relation to the variation that occurred in $\omega^{(l)}$ in the anterior instant, $\partial\omega^{(l)}$. Therefore, using the chain rule to calculate $\partial E/\partial\omega^{(l)}$ results in expression (21).

$$\frac{\partial E}{\partial \omega^{(l)}} = \frac{\partial E}{\partial Y}\frac{\partial Y}{\partial a}\frac{\partial a}{\partial \omega^{(l)}} \tag{21}$$

The use of chain rule looks for the term contained in E that is directly dependent on the value to be adjusted, i.e., the conclusion value $\omega^{(l)}$. Therefore, we can verify by chain equation (21) that it starts with E dependent of Y value, the Y value depends on term α and, at last, the expression a is a function of $\omega^{(l)}$. After some computation, the adjustment to be made in $\omega^{(l)}$ can be interpreted as being proportional to the error between the neuro-fuzzy model response and the supervising value, but weighted by the contribution of rule (l), denoted by $d^{(l)}$, to the final neuro-fuzzy inference.

$$\omega^{(l)}(t+1) = \omega^{(l)}(t) - \alpha\frac{(Y(x^{'}(k)) - y^{'}(k))d^{(l)}}{\sum\limits_{l=1}^{c}(d^{(l)})} \tag{22}$$

Next, a convergence theorem has been developed to guarantee the stability of learning algorithm used for the above-mentioned FNN [14]. A lyapunov energy function is defined as follows:

$$V_k = J_k = \frac{1}{2} E_k^2.$$

(23)

From equation (23), we can get

$$\Delta V = V_{k+1} - V_k = \frac{1}{2}(E_{k+1}^2 - E_k^2).$$

(24)

The error difference, ΔE_k, can be defined as

$$\Delta E_k = E_{k+1} - E_k = \frac{\partial E_k}{\partial \omega} \Delta \omega,$$

(25)

where $\Delta \omega = \omega_{k+1} - \omega_k = -\alpha E_k \frac{\partial E_k}{\partial \omega}$

(26)

Using equation (24), we can get

$$\Delta V = \frac{1}{2}(E_{k+1} - E_k)(E_{k+1} + E_k)$$

$$= \frac{1}{2}(\Delta E_k)(2E_k + \Delta E_k).$$

(27)

Substituting equation (26) into equation (27), we have

$$\Delta V = \frac{1}{2} \frac{\partial E_k}{\partial \omega} \alpha E_k \frac{\partial E_k}{\partial \omega}(-2E_k + \frac{\partial E_k}{\partial \omega} \alpha E_k \frac{\partial E_k}{\partial \omega})$$

$$= \frac{1}{2}(E_k \frac{\partial E_k}{\partial \omega})^2 \left[(\frac{\partial E_k}{\partial \omega})^2 \alpha^2 - 2\alpha \right].$$

(28)

If $\Delta V < 0$, the convergence of the algorithm described in equation (28) can be guaranteed. Therefore, we have

$$\left(\frac{\partial E_k}{\partial \omega} \right)^2 \alpha^2 - 2\alpha < 0.$$

(29)

From equation (29), we can obtain

$$0 < \alpha < \frac{2}{\left(\frac{\partial E_k}{\partial \omega} \right)^2}$$

(30)

3.2. Control of Fuel Cell Subsystem

The fuel cell reference power is generated as the difference between the load power demanded minus the PV power. An additional power proportional to the difference of battery reference voltage and the current battery voltage is generated by an outer loop voltage controller to charge the battery. This additional power is then added to the fuel cell reference power demanded from the load to generate the overall fuel

cell power reference. A proportional controller is sufficient for batteries with flat voltage profiles as in Li-ion battery. Fig.7 shows the control strategy of the fuel cell subsystem.
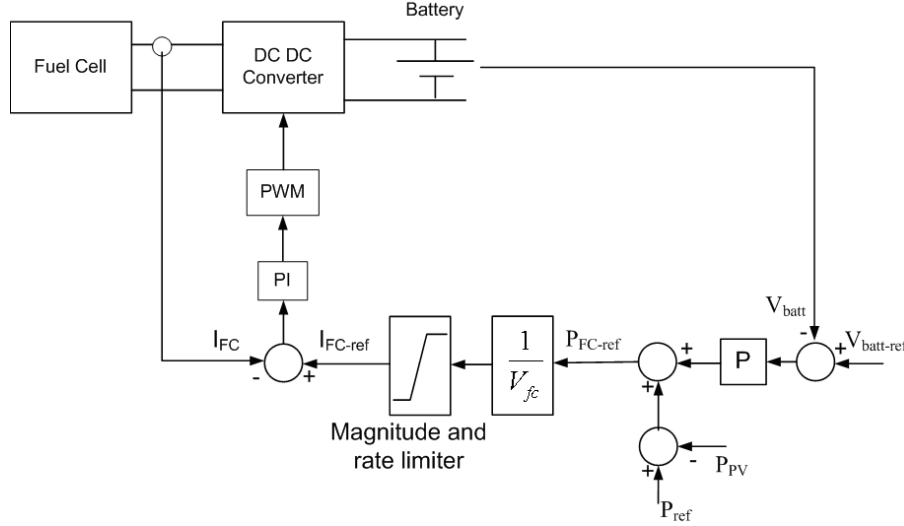

Fig. 7.Control of fuel cell subsystem

In order to design control strategy for fuel cell power plant, two parameters should be considered and regulated. These parameters are hydrogen flow according to output power and fuel cell current. According to the equations (2) and (3), to control hydrogen flow from the fuel cell, a feedback from the stack current is considered. Equation (3) shows that the reacting fuel quantity, $q_{H_2}^r$, is directly proportional to the output current, I_{fc}, the factor K_r being a cell constant. Hence, the desired utilization is translated to corresponding output current demand:

$$q_{H_2}^{in} = \frac{2K_r}{U_{f,opt}} I_{demand} \qquad (6)$$

A proportional integral (PI) controller is used to control the flow rate methane in the reformer. Oxygen flow is determined using the hydrogen-oxygen flow ratio r_{H-O}. The control strategy for reformer is illustrated in Fig.3.

In the proposed control structure, choosing the control system parameters affects the system performance. So it is important to design PI controller properly. Another important parameter that must be controlled properly is fuel cell current. For this purpose, a boost DC-DC converter is selected for fuel cell converter. The current mode control of DC-DC converter has been used to regulate the fuel cell current. A typical range of U_f is 80-90% [4], which ensures that the operational limits mentioned above are observed. The corresponding limitation for the demand current is then calculated as following equation:

14

$$\frac{0.8q_{H_2}^{in}}{2K_r} = I_{fc\_min} \leq I_{fc\_ref} \leq I_{fc\_max} = \frac{0.9q_{H_2}^{in}}{2K_r} \qquad (7)$$

To obtain transfer function of fuel cell current loop and apply classical control analysis and design methods (such as Nyquist criterion, Bode plots) in converter controls, the following transfer function can be investigated based on the state space signal models of boos DC-DC converter model [3,16]:

$$T_{i_{FC-d}}(s) = \frac{i_{FC}(s)}{d(s)} = \frac{1}{s^2 + \dfrac{R_L}{L}s + \dfrac{(1-D)^2}{LC}} [s(\frac{V_{CO}}{L}) + \frac{I_{LO}(1-D)}{LC}] \qquad (8)$$

The control structure for fuel cell current with has been shown in Fig.4. In this structure, the transfer function of PWM block can be modeled as:

$$T_{PWM} = \frac{1}{K_{PWM}} \qquad (9)$$

3.3. Control of Grid Connected Voltage Source Converter

Control of grid connected voltage source converter is an important problem during voltage disturbances. It needs fast current controllers to track the current references according to change in active and reactive power during the fault. The current controller used in this paper consists of two vector current controllers based on Sliding Mode Control (SMC) that regulate the positive and negative sequence currents separately and are implemented in two different rotating coordinate systems. The need for regulating the positive and negative sequence currents is related for treating the unbalance voltage conditions.

A simplified scheme for the proposed control strategy is shown in Fig.9. The three phase grid currents and voltages are sampled and transformed into its positive and negative sequence components. The positive and negative sequence of dq-components are then used along the with the reference current signals to produce the reference voltage signals for the PWM regulator. A sequence separation method (SSM) is needed to extract positive and negative sequences. Delayed Signal Cancellation method (DSC) is probably the best suited SSM [10]; but produces transient oscillations at the start and end period of voltage sag [5]. The layout of this method is illustrated in Fig.10. The abc system is first transformed into stationary αβ reference frame using Clark's transformation, and then it is delayed for T/4. The positive and negative sequences can be calculated by adding or subtracting the present real-time signal with delayed signal in the following way:

$$\begin{pmatrix} v_\alpha^p(t) \\ v_\beta^p(t) \\ v_\alpha^n(t) \\ v_\beta^n(t) \end{pmatrix} = \frac{1}{2} \begin{bmatrix} 1 & 0 & 0 & -1 \\ 0 & 1 & 1 & 0 \\ 1 & 0 & 0 & 1 \\ 0 & 1 & -1 & 0 \end{bmatrix} \begin{pmatrix} v_\alpha(t) \\ v_\beta(t) \\ v_\alpha(t - \dfrac{T}{4}) \\ v_\beta(t - \dfrac{T}{4}) \end{pmatrix} \tag{15}$$

According to the proposed control strategy, the purpose of the current controller is to synthesize a voltage correction vector so that the current error vector can be kept to a minimum value.

In this paper, the current controller has been implemented by using SMC technique due to its robustness and overshoot-free fast tracking capability [20].

The SMC is a nonlinear control approach which complies with the nonlinear characteristic of a power electronic converter. Such control technique is robust even against the plant parametric variation and can compensate the modeling approximations. Also, it is characterized by a good dynamic response. In addition, the SMC is simple to implement.

According to the dynamic model of inverter given in (14), the state space equations of the system can be written as (16).

$$\dot{X}(t) = AX(t) + BU + EV_g$$
$$Y(t) = CX(t) \tag{16}$$

where the state variable is X, the control input U and grid voltage V_g and given in (17-19).

$$X = \begin{bmatrix} i_{2d}^p & i_{2q}^p & i_{2d}^n & i_{2q}^n \end{bmatrix}^T \tag{17}$$

$$U = \begin{bmatrix} U_d^p & U_q^p & U_d^n & U_q^n \end{bmatrix}^T \tag{18}$$

$$V_g = \begin{bmatrix} V_{gd}^p & V_{gq}^p & V_{gd}^n & V_{gq}^n \end{bmatrix}^T \tag{19}$$

For the control plant given in (16), the sliding mode control law can be derived as follows. To let the current output Y track the reference input i_{ref}, a sliding mode manifold can be chosen in the form of (20).

$$\begin{bmatrix} S_p^{dq} \\ S_n^{dq} \end{bmatrix} = \begin{bmatrix} i_{2dq}^p \\ i_{2dq}^n \end{bmatrix} - \begin{bmatrix} i_{2dq}^{p,ref} \\ i_{2dq}^{n,ref} \end{bmatrix} \tag{20}$$

Where $i_{2dq}^{p,ref}$ and $i_{2dq}^{n,ref}$ are the specified current vector commands for the positive and negative sequence of dq-components.

The sliding mode can be reached if the control input $U(t)$ is designed to be the solution of (21):

16

$$\frac{d}{dt}S(t) = 0 \tag{21}$$

The control law satisfies (21) is called equivalent control and is given by (22)

$$U_{eq}(t) = (CB)^{-1}[i_{ref} - CAX(t) - CEV_g(t)] \tag{22}$$

In order to generate proper current references, consider the complex apparent power from the grid:

$$S_g = (v_{sdq}^p e^{j\omega t} + v_{sdq}^n e^{-j\omega t}).(i_{2dq}^p e^{j\omega t} + i_{2dq}^n e^{-j\omega t})^* =$$
$$(P + P_{2c}.\cos(2\omega t) + P_{2s}.\sin(2\omega t)) + \tag{23}$$
$$j(Q + Q_{2c}.\cos(2\omega t) + Q_{2s}.\sin(2\omega t))$$

By expanding (23), the following expression in matrix form can be written:

$$P = (v_{sd}^p.i_{2d}^p + v_{sq}^p.i_{2q}^p + v_{sd}^n.i_{2d}^n + v_{sq}^n.i_{2q}^n)$$
$$Q = (v_{sq}^p.i_{2d}^p - v_{sd}^p.i_{2q}^p + v_{sq}^n.i_{2d}^n - v_{sd}^n.i_{2q}^n)$$
$$P_{c2} = (v_{sd}^p.i_{2d}^n + v_{sq}^p.i_{2q}^n + v_{sd}^n.i_{2d}^p + v_{sq}^n.i_{2q}^p)$$
$$P_{s2} = (v_{sd}^p.i_{2q}^n - v_{sq}^p.i_{2d}^n - v_{sd}^n.i_{2q}^p + v_{sq}^n.i_{2d}^p) \tag{24}$$
$$Q_{c2} = (v_{sq}^p.i_{2d}^n - v_{sd}^p.i_{2q}^n - v_{sd}^n.i_{2q}^p + v_{sq}^n.i_{2d}^p)$$
$$Q_{s2} = (v_{sd}^p.i_{2d}^n + v_{sq}^p.i_{2q}^n - v_{sd}^n.i_{2d}^p - v_{sq}^n.i_{2q}^p)$$

Where P and Q are the constant active and reactive power, respectively, while the subscripts P_{s2} and P_{c2} represent the second harmonic sine and cosine component of the active power. These are the oscillating active powers due to the unbalance in the grid voltages. During generating the reference currents, the oscillating reactive powers (Q_{2c}, Q_{2s}) cannot be included in the calculation. Therefore to simplify the calculation and work with an invertible matrix (4×4), oscillating reactive power is not controlled and will flow through the system [5].

Hence, the reference currents can be calculated as follow:

17

$$\begin{bmatrix} i_{2d}^{p*} \\ i_{2q}^{p*} \\ i_{2d}^{n*} \\ i_{2q}^{n*} \end{bmatrix} = \begin{bmatrix} v_{sd}^{p} & v_{sq}^{p} & v_{sd}^{n} & v_{sq}^{n} \\ v_{sq}^{p} & -v_{sd}^{p} & v_{sq}^{n} & -v_{sd}^{n} \\ v_{sq}^{n} & -v_{sd}^{n} & -v_{sq}^{p} & v_{sd}^{n} \\ v_{sd}^{n} & v_{sq}^{n} & v_{sd}^{p} & v_{sq}^{p} \end{bmatrix}^{-1} \begin{bmatrix} P^* \\ Q^* \\ -\Delta P_{s2} \\ -\Delta P_{c2} \end{bmatrix} \tag{25}$$

$$\Delta P = 2 \times (R_1 + R_2) \times ((i_{2d}^p)^2 + (i_{2q}^p)^2 + (i_{2d}^n)^2 + (i_{2q}^n)^2) \tag{26}$$

$$\Delta P_{c2} = 2 \times (R_1 + R_2) \times (i_{2d}^p.i_{2d}^n + i_{2q}^p.i_{2q}^n) + 2 \times \omega \times L \times (i_{2d}^p.i_{2q}^n - i_{2q}^p.i_{2d}^n) \tag{27}$$

$$\Delta P_{s2} = 2 \times (R_1 + R_2) \times (i_{2d}^p.i_{2q}^n - i_{2q}^p.i_{2d}^n) + 2 \times \omega \times (L_1 + L_2) \times (-i_{2d}^p.i_{2d}^n - i_{2q}^p.i_{2q}^n) \tag{28}$$

This algorithm calculates current references by setting active and reactive power references (P^*, Q^*), and by forcing the oscillating active power demanded by the filter to be delivered from the grid ($P_{2c}^* = -\Delta P_{2c}$; $P_{2s}^* = -\Delta P_{2s}$). Then, no oscillating active power flows between the dc link and the filter.

The phase locked loop (PLL) estimates the grid voltage phase angle which is then used to synchronize the inverter output voltage to the grid.

4. Simulation Results

To evaluate the effectiveness of the proposed control strategy, the system is simulated in SIMULINK/SIMPOWER over a 100sec of real and reactive load profiles.

The choice of the DC-bus voltage depends on the output voltage of the inverter required which should give the grid voltage. The relationship between the DC link voltage V_{dc} and the line-to-line RMS grid voltage $V_{LL,AC}$, where m_a is the modulation index in the linear region, is given in (23)[24].

$$V_{dc} \geq \frac{1.633}{m_a} V_{LL,AC} + voltage drops \tag{23}$$

Assuming filter impedance drop of 5% of grid voltage and to give an output voltage of 400V at PCC, the nominal DC-link voltage was chosen at 720V.

Seven strings of each 16 series modules are used to provide a PV peak capacity of around 25kWp. The PV modules are the same as the one modeled in section II. To test how the control strategy reacts for a varying PV output profile, the irradiance over 300sec was assumed to have variation.

18

Twenty one 1.2kW, 12-21V PEMFC stacks which are the same as the one modeled in section II were stacked in series to provide 25kW power at rated operation. This provides a full back up to the PV during zero PV output. At rated operation the fuel cell stack voltage at the input to the boost converter is 21x12V=252V.

A 11Ah Li-ion battery bank stacked out of the same cells modeled in section II is used to form the DC-link. This battery bank has a full charge voltage of around 726V and a 50% SOC voltage of 710V. This voltage band is sufficiently within the inverter operating area. The flat voltage profile of the battery bank is controlled from the DC side as explained in *III.B*.

Figs. 9 and 10 show the active and reactive load powers and the power delivered from the hybrid power and the grid. Both show that balance of power is satisfied. All the reactive power demand is supplied locally from the hybrid power system enabling the grid to operate at unity power factor. From 50 to 200sec, where the capacity of the hybrid power system is exceeded, the remaining 10kW of the active power is supplemented by the grid. For the rest of the profile where the load is less than or equal to 40kW, all the demand is covered by the hybrid power system.
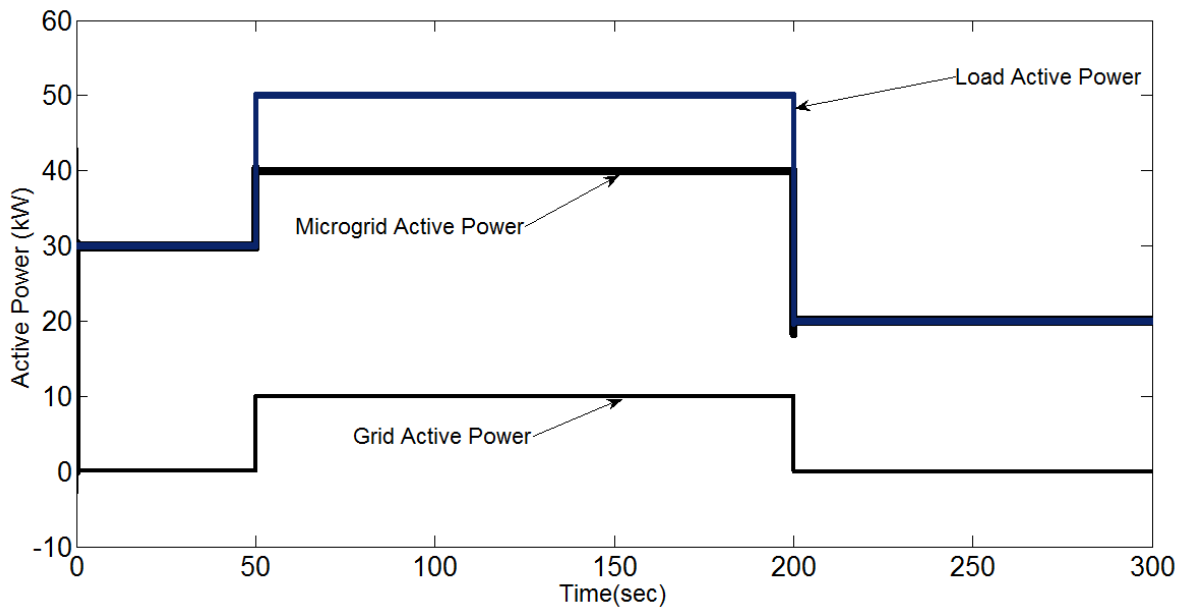
Fig.9 Active load, microgrid and grid power
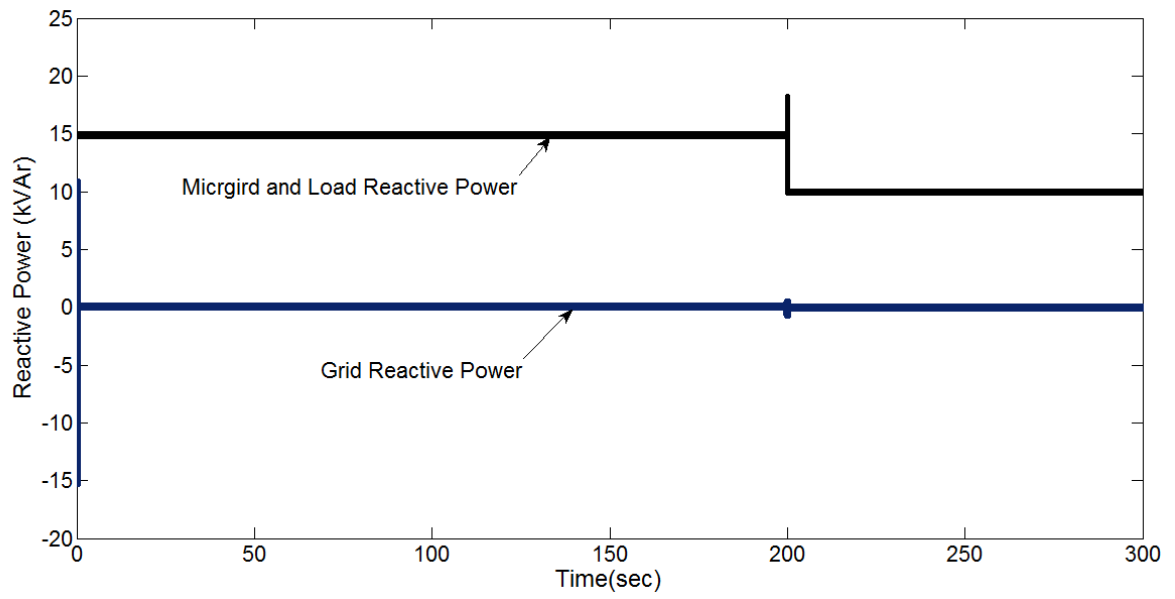
Fig.10 Reactive load, microgrid and grid power
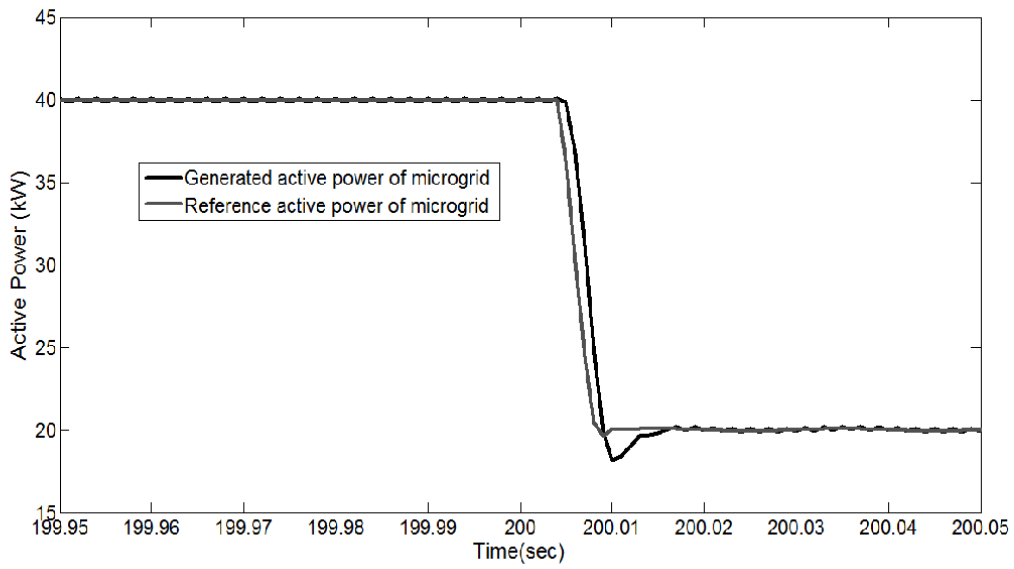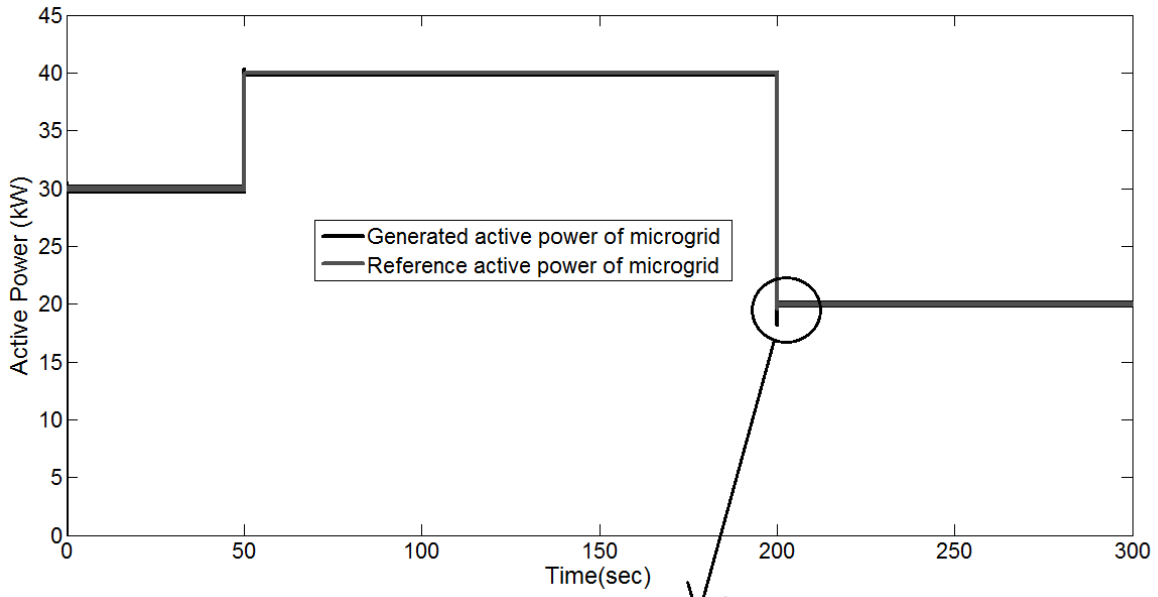
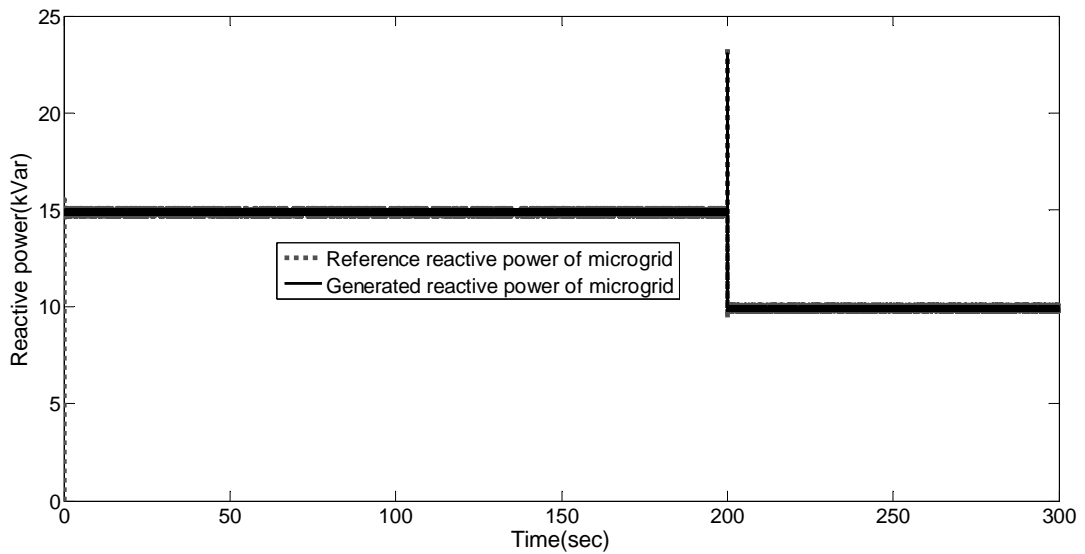Fig.11 Generated and reference active power of Microgrid

Fig.12 Generated and reference reactive power of Microgrid

Figs. 11 and 12 give the microgrid power tracking performance of the inverter controller. It is seen that the controller quickly tracks the reference powers with only small overshoot.

Fig.13 shows the load current sharing between the different power sources and energy storage all referred to the DC-link. Initially, the load active power is supplied from the PV and the fuel cell. Since the initial battery state of charge is 75%, the fuel cell controller requests additional charging power to the battery depending on the difference between the DC-link reference voltage and the battery voltage. At t=50sec, the active load power suddenly increases from 20kW to 50kW and stays for the next 200seconds. At first the battery responds to the instant transient by quickly decreasing its charging current while the fuel cell steadily goes to its maximum output (25kW). Since the maximum capacity (including the battery peak shaving capacity) is only 40kW, the rest 10kW of load power is provided by the grid. From 150 to 200sec, the PV output is very low and the rest of the 40kW microgrid power is provided by the battery. After 200s the PV output increases and the battery current decreases eventually going to charging mode. Starting from 250sec, the fuel cell begins to save fuel and decreases its output since the battery goes to full charge reference voltage of 720V.
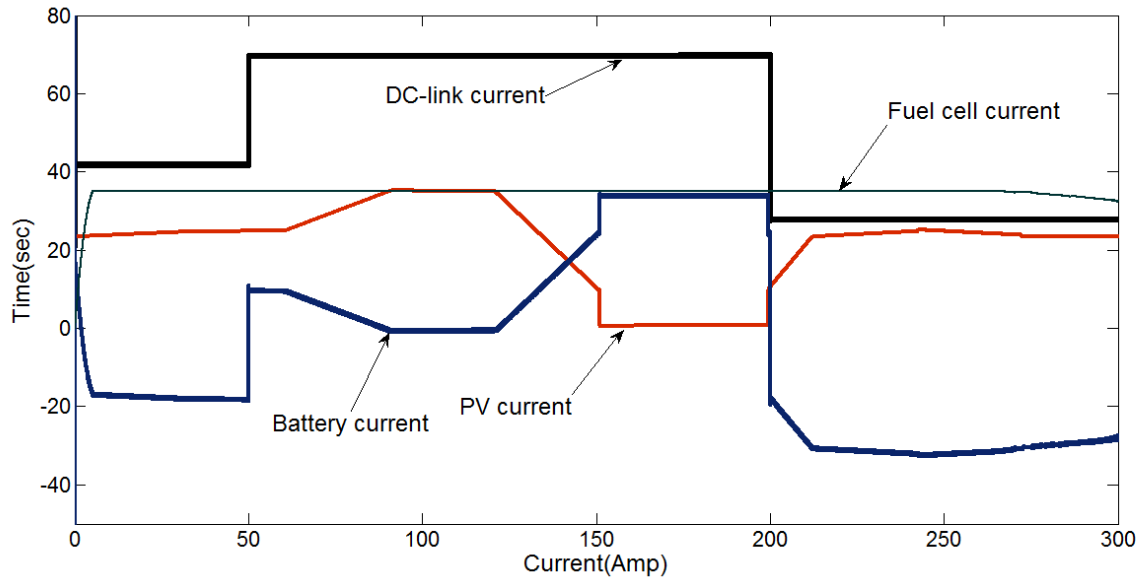
22

Fig.13 DC-link, PV, Fuel cell and Battery Current

Fig. 14 shows the battery voltage during the whole power profile. As shown, the power flow control strategy on the DC side always keeps the DC-link voltage within the reasonable range for the inverter. Fig.15 shows the *dq* sequence components of the injected currents by the inverter. As shown, the fast action of the proposed controller in supplying the power to the grid is obvious.
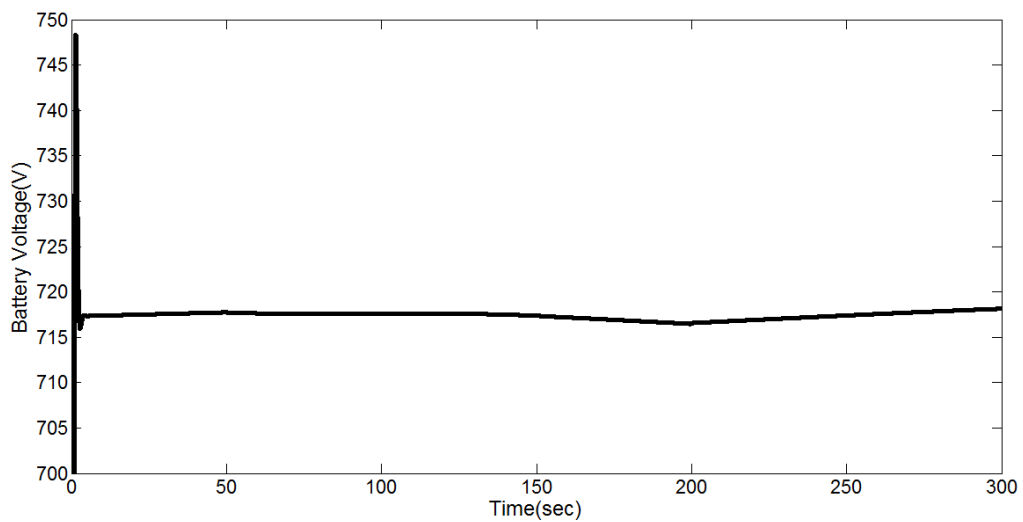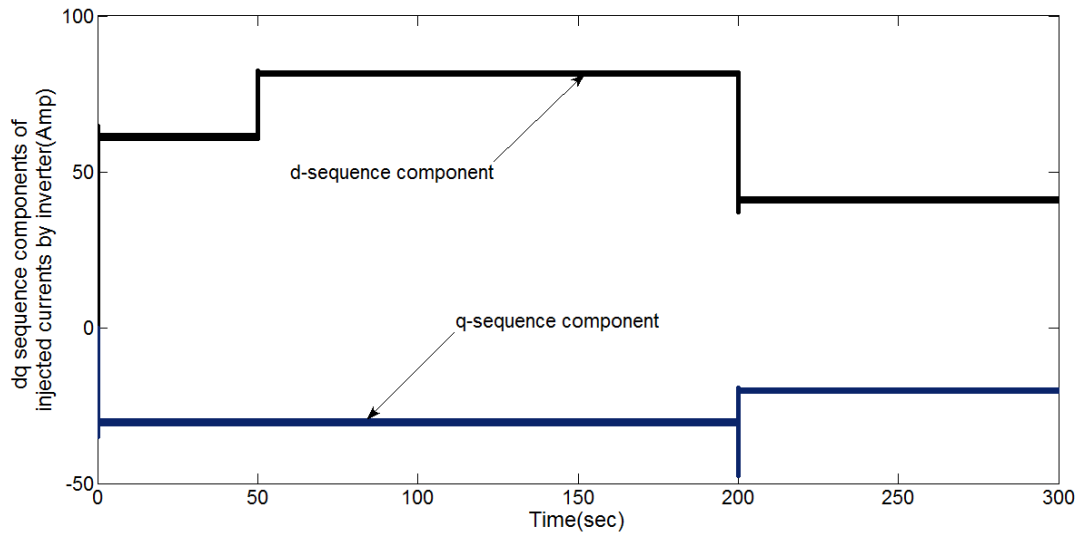

Fig. 14 Battery Voltage

Fig.15 dq sequence components of injected currents by inverter

In order to show the response of the power control strategy during the unbalanced voltage condition, another simulation results have been extracted. In this case, The proposed control strategy has been examined in case of unbalanced voltage conditions. An unbalanced voltage, resulting from unbalanced load, is applied at the grid side. The unbalanced voltage starts at 1.2 sec for duration of 2 sec. The grid voltage during unbalanced voltage has been shown in Fig.16.
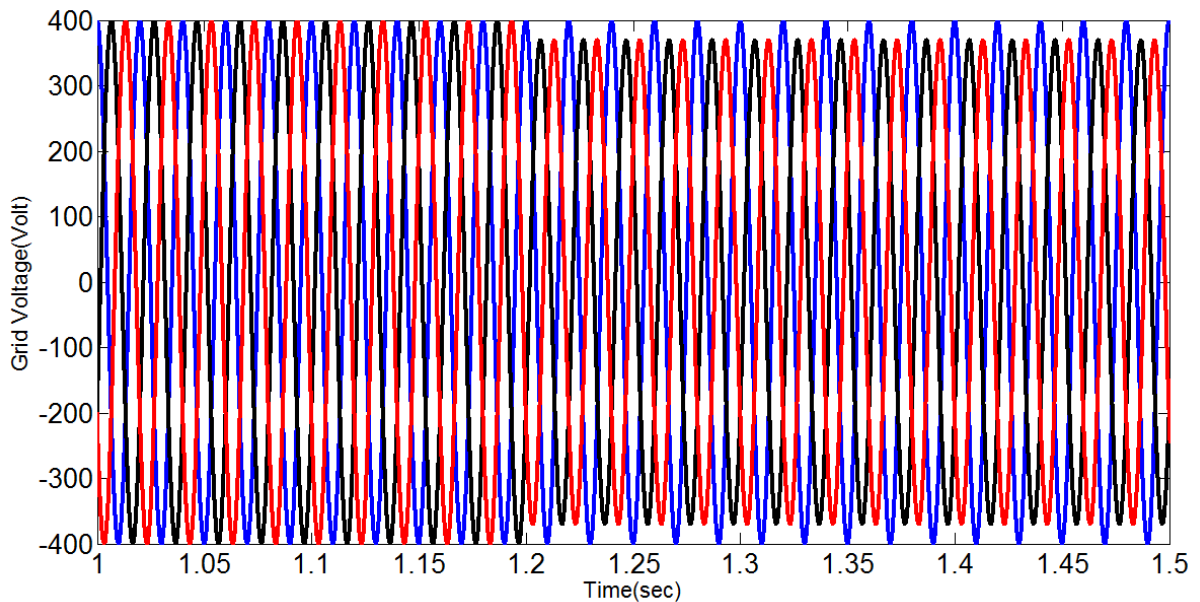
Fig.16 the unbalanced grid voltages

In Fig.17 , the average and instantaneous active power during normal and unbalanced voltage conditions have been presented. As shown during unbalanced voltage, there are small oscillations on instantaneous active power. These oscillations are related to the proposed current control strategy that considered in this paper. It makes the oscillating active power that demands by the filter to be delivered from the grid. In this case no oscillating active power flows between the DC link and the filter.
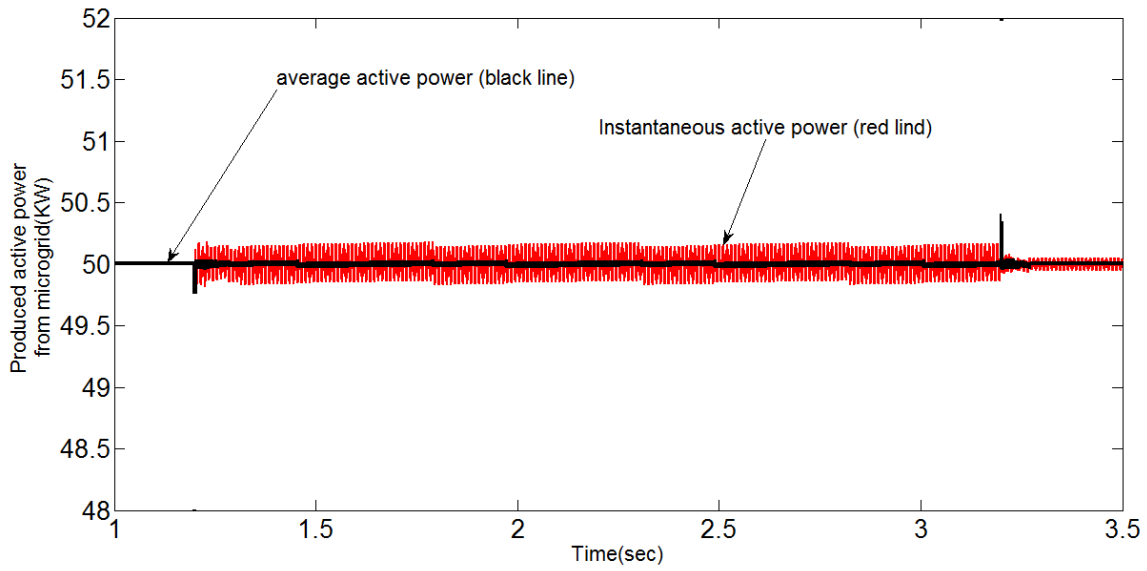

Fig.17 average and instantaneous active power of microgrid

Moreover, there are large oscillations on reactive power that is shown in Fig.18. But the average of reactive power is 5KVar.
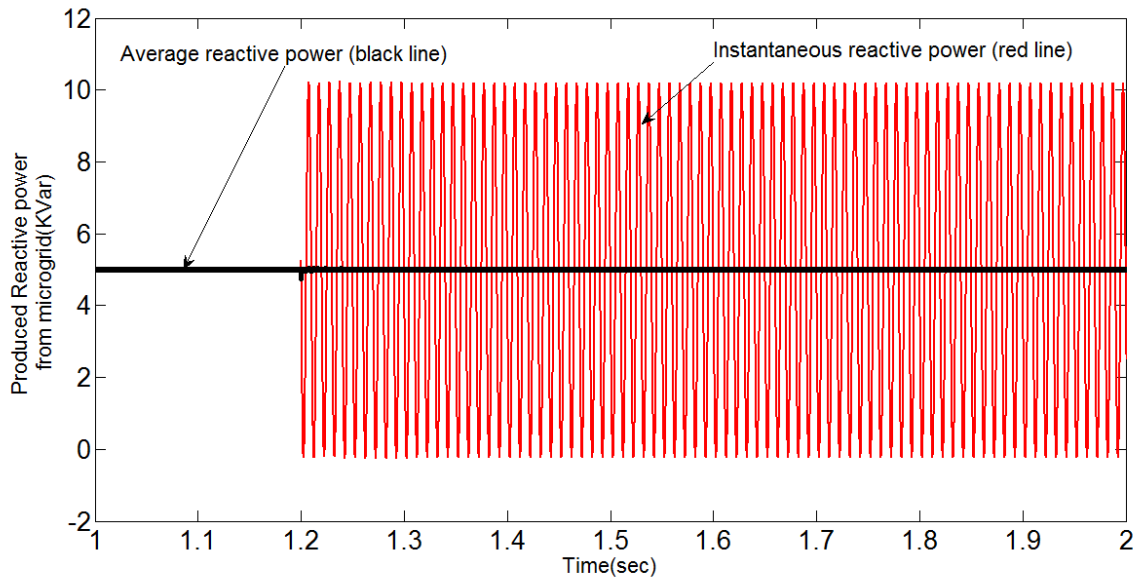
Fig.18 average and instantaneous reactive power of microgrid

The DC link voltage is shown in Figs.19. During the unbalanced voltage, there is an increase on DC link voltage but it is not much more than 10% of nominal value. In these conditions, to stabilize the dc-link power, the neuor-fuzzy controller manages the power flow between power sources.
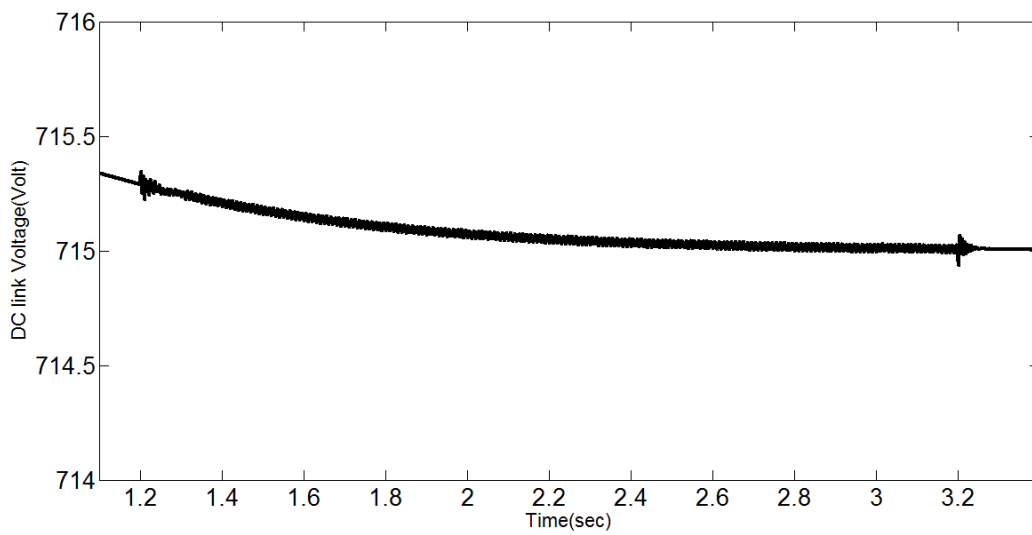

Fig.19 DC-link voltage

26

To evaluate the voltage regulation performance under unbalanced grid voltage conditions due to a sudden load change, the proposed dual-sequence voltage controller has been tested. Figure 23 shows the grid voltage at the PCC during unbalanced voltage sag.
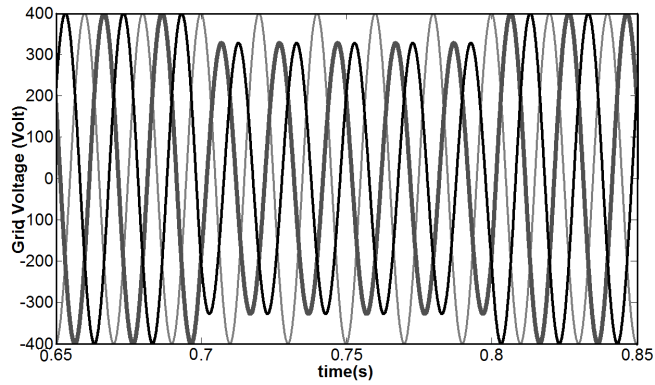

Fig.23 Grid voltage at the PCC during unbalanced voltage sag

Figures 24 and 25 depict the control performance of the proposed scheme under the unbalanced grid voltage type C with magnitude 90%. Fig. 26 shows the 3-phase voltages; which are well regulated under the unbalanced disturbance.
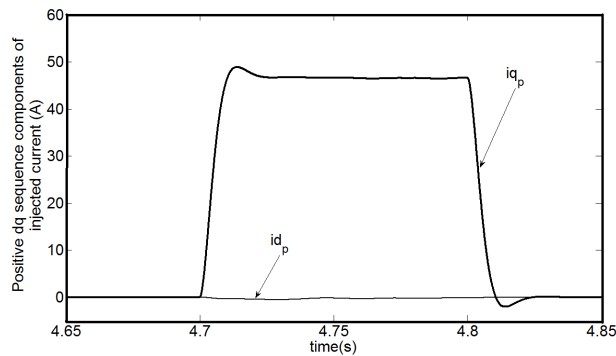

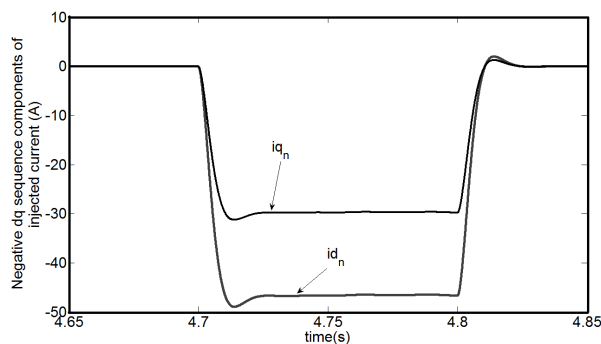Fig.24 Positive dq sequence components of injected currents by voltage source converter

Fig.25 Negative dq sequence components of injected currents by voltage source converter
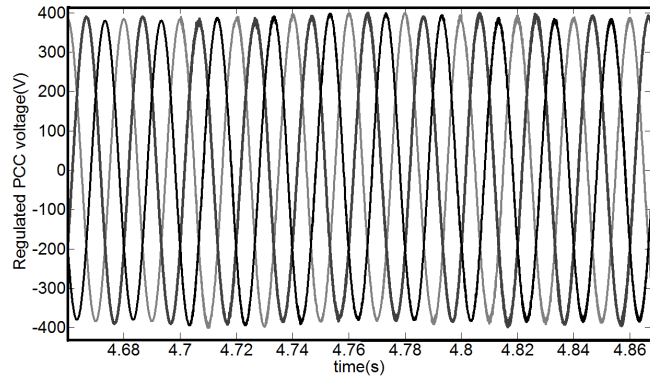
Fig.26 Regulated grid voltage

Fig.27 shows the positive sequence *dq* components of the grid voltage, whereas Fig.28 shows the corresponding negative sequence components. Since the inverter interface is supporting the grid reactively in a fast manner, only the *d*-component of the positive sequence grid voltage appears, whereas other sequence components vanish swiftly. The fast action of the proposed controller in regulating the line voltage is obvious. Moreover, the amount of average and instantaneous reactive power is injected to grid to regulate the voltage at the PCC, is presented in Fig.29.

As illustrated, there is a limitation to inject more reactive power for more voltage drop to compensate the voltage at the PCC. Also, the extent to which a DG can help the grid to regulate its voltage depends on the DG capacity and the grid capacity.

So, the proposed voltage control strategy for this system could not mitigate all kind of voltage sag with more voltage drop than 85%.
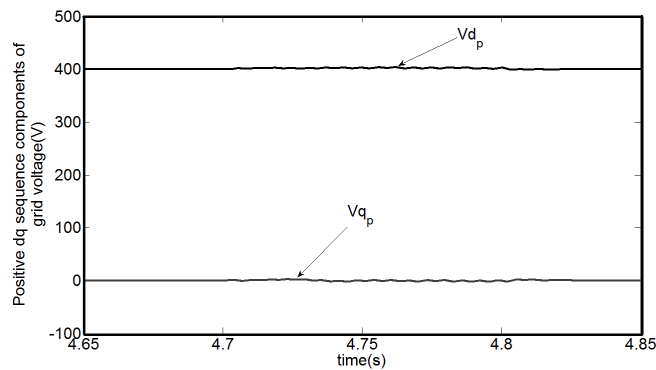

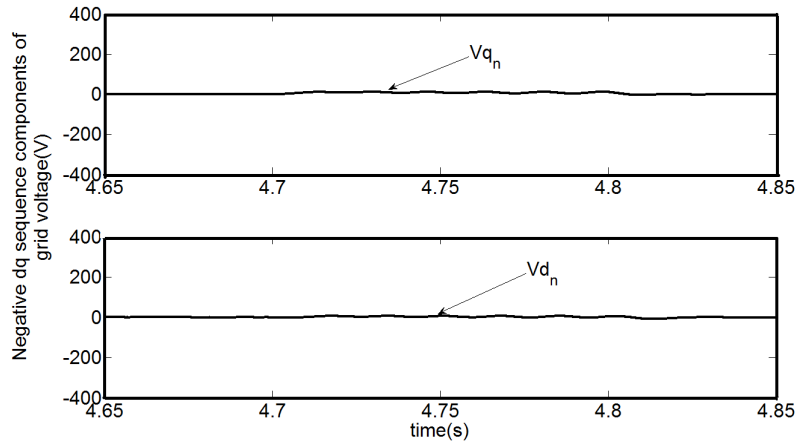Fig.27 Positive dq sequence components of grid voltage

28

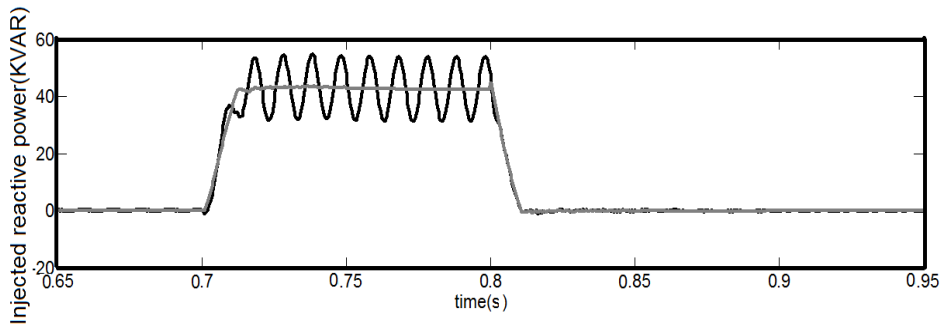Fig.28 Negative dq sequence components of grid voltage

Fig.29 Injected reactive power during voltage sag type C

5. Conclusion

This paper presents modeling, control and power control in a grid connected PV/Fuel Cell/Battery hybrid power generation system in a microgrid. SIMULINK/SIMPOWER was used to model the system and simulate a power flow control strategy. PV, fuel cell and battery subsystems with power electronic converters are modeled. Then control strategies are designed for power electronic converters based on the classic and fuzzy –sliding mode control. It was shown that the microgrid can be controlled as desired to follow the local demand and allow the grid to operate at or near unity power factor. To distribute the power between power sources, the neuro-fuzzy power sharing controller has been developed. Simulation results are presented to demonstrate the effectiveness of the control strategy.

References

[1] R. H. Lasseter, "MicroGrids" in Proc.IEEE Power Engineering Society Winter Meeting, Vol. 1, pp. 305-308, 2002.

[2] M. W. Davis, "Distributed resource electric power systems offer significant advantages over central station generation and T&D power systems, part I," in *IEEE T&D Conference and Exposition*, Atlanta, Georgia, Oct./Nov. 2001, pp. 54–61.

[3] R. H. Lasseter and P. Piagi, "MicroGrid: A conceptual solution", in Proc. Power Electronics Specialists Conference, Aachen, Germany, June 2004, vol. 6, pages: 4285–4290.

[4] F. Katiraei, M.R. Iravani, "Transients of a Micro-Grid System with Multiple Distributed Energy Resources", International Conference on Power Systems Transients (IPST'05) in Montreal, Canada on June 19-23, 2005.

[5] Amin Hajizadeh, Masoud Aliakbar Golkar, "Intelligent Power Management Strategy of hybrid Distributed Generation System", International Journal of Electrical Power and Energy Systems 29 (2007) 783–795.

[6] H. Habeebullah Saita, S. Arul Daniel, "New control paradigm for integration of photovoltaic energy sources with utility network", International Journal of Electrical Power & Energy Systems, 33 (2011) 86-93.

[7]Amin Hajizadeh, Masoud Aliakbar Golkar, "Control of Hybrid Fuel Cell/Energy Storage Distributed Generation System against Voltage Sag", International Journal of Electric Power and Energy Systems, 32 (2010) 488-497.

[8] Ramon Zamora, Anurag K. Srivastava, "Controls for microgrids with storage: Review, challenges, and research needs", Renewable and Sustainable Energy Reviews, ELSEVIER, (2010).

[9] Ali Mehrizi-Sani, Reza Iravani, "Potential-Function Based Control of a Microgrid in Islanded and Grid-Connected Modes", IEEE TRANSACTIONS ON POWER SYSTEMS, 2010.

[10] Amin Hajizadeh, Masoud Aliakbar Golkar, "Fuzzy Control of Fuel Cell Distributed Generation Systems", Iranian Journal of Electrical & Electronic Engineering (IJEEE), Vol.13, No 1& 2, Jan. 2007.

[11]Milan Prodanovic and Timothy C. Green, "Control and Filter Design of Three-Phase Inverters for High Power Quality Grid Connection", IEEE TRANSACTIONS ON POWER ELECTRONICS, VOL. 18, NO. 1, JANUARY 2003.

[12] T.C. Green, M.Prodanovic, "Control of inverter-based micro-grids", Electric Power Systems Research (2006)

[13] Milan Prodanovic and Timothy C. Green,"High-Quality Power Generation Through Distributed Control of a Power Park Microgrid", IEEE TRANSACTIONS ON INDUSTRIAL ELECTRONICS, VOL. 53, NO. 5, OCTOBER 2006.

[14] Yunwei Li, D. Mahinda Vilathgamuwa,Poh Chiang Loh, "Microgrid Power Quality Enhancement Using a Three-Phase Four-Wire Grid-Interfacing Compensator", IEEE TRANSACTIONS ON INDUSTRY APPLICATIONS, VOL. 41, NO. 6, NOVEMBER/DECEMBER 2005.

[15] Yunwei Li, D. Mahinda Vilathgamuwa,Poh Chiang Loh,"A Grid-Interfacing Power Quality Compensator for Three-Phase Three-Wire Microgrid Applications", IEEE TRANSACTIONS ON POWER ELECTRONICS, VOL. 21, NO. 4, JULY 2006.

[16] M.Y.El-Sharkh, A.Rahman, M.Y.Alam, P.C.Byrne, A.A.Sakla, T.Thomas, "A dynamic model for a stand-alone PEM fuel cell power plant for residential applications", Journal of Power Sources, vol.138, pp.199-204,2004.

[17] C. M. J.A. Gow, Development of a photovoltaic array model for use in power-electronics simulation studies," in Electric Power Applications, IEE Proceedings, vol. 146, pp. 193{200, March 1999.

[18] M. F Ishengoma and L. E Norum. Design and implementation of a digitally controlled stand-alone photovoltaic power supply. In Nordic Workshop on Power and Industrial Electronics (Norpie 2002), Stockholm, Sweden, 12-14 Aug. 2002.

[19] K. Hussein, I. Muta, T. Hoshino, and M. Osakada, "Maximum photovoltaic power tracking: an algorithm for rapidly changing atmospheric conditions", Generation, Transmission and Distribution, IEE Proceedings. vol. 142, pp. 59,Jan 1995.

[20] D. Hohm and M. Ropp, "Comparative study of maximum power point tracking algorithms using an experimental, programmable, maximum power point tracking test bed" Photovoltaic Specialists Conference, 2000. Conference Record of the Twenty-Eighth IEEE, pp. 1699-1702, 2000.

[21] B.Yuri, YB.Shtessel, A.Zinober, A.Shkolnikov," Sliding mode control of boost and buck-boost power converters using method of stable system centre", Automatica, vol.39, pp.1061–1067, 2005.

[22] Amin Hajizadeh, Masoud Aliakbar Golkar, "Intelligent Robust Control of Hybrid Distributed Generation System under Voltage Sag", Journal of Expert Systems with Applications, 37 (2010) 7627–7638.

[23] J.J. Slotine and W. Li, Applied Nonlinear Control (Prentice-Hall, Englewood Cliffs, NJ, 1991).

[23] N. Mohan, T.M. Undeland, W.P. Robbins, Power Electronics Converters,Applications and Design (Wiley, 2003).